BL7U

Direct Measurements of Metallic Property of Organic Materials upon Temperature-Dependent Photoelectron Spectroscopy

X. Liu[1], J. P. Yang[2], K. Tanaka[3], H. Tang[4], F. Huang[4], S. Kera[3] and M. Fahlman[1]

[1]*Laboratory of Organic Electronics, ITN, Linköping University, Norrköping SE-60174, Sweden*

[2]*College of Physical Science and Technology, Yangzhou University, Jiangsu 225009, China*

[3]*UVSOR Synchrotron Facility, Institute for Molecular Science, Okazaki 444-8585, Japan*

[4]*Institute of Polymer Optoelectronic Materials and Devices, State Key Laboratory of Luminescent Materials and Devices, South China University of Technology (SCUT), Guangzhou, China*

Engineering electronic properties of pi-conjugated polymers upon functional groups from material synthesis to post-treatment with external dopants is of vital importance for the development of air stable, soluble, effective charge transport materials on organic devices [1]. Doping induced delocalization of (bi) polarons and their intra-chain carrier transport in pi-conjugated polymers is the basis of the field of "organic synthetic metals", as well as the foundation of modern organic electronic devices. For instance, PEDOT:PSS, are commercially available hole-dominant (p-type doping) materials with conductivity up to several thousand S/cm, which can be labelled as semi-metallic polymer [2] with no energy gap and very low density of states (like tail states) at the Fermi level due to the contribution of high (bi)polaron density. The information related to the high-conducting n-type (electron-dominant) ones is rather less, e.g., there is still controversy about the new states near the Fermi level of K-doped picene [3], related to the semiconductor-metal transition. Recently, the successful synthesis of air-stable, soluble, and high conducting n-type polymer PBFDO ($(C_{10}O_4H_4)_n$, shown in the inset of Fig. 1(b)) shows the electron conductivity up to 2000 S/cm and very deep LUMO (lowest unoccupied molecular orbitals) [4]. It is believed that the PBFDO is at the critical regime of Mott transition by n-type self-doping with 0.9 electron per unit during polymerization process while the presence of protons in the solvent was used to balance the negative charge. We carried out a UPS study of our-synthesized PBFDO film, a clear Fermi edge feature on free-standing PBFDO films was obviously visible with a work function of up to 5.4 eV, like clean Pt or Au metals.

Any information related to clear Fermi edge feature in high-conducting organic synthetic metals from photoelectron spectroscopy will offer solid evidence of their metallic properties, but it is missing yet for PBFDO. The temperature-dependent Fermi edge features can provide a test about applying Tomonaga–Luttinger liquid or Fermi liquid/glass theory to electronic transport properties of organic synthetic metals.

In this study, we examined the valence band feature of PBFDO close to the Fermi edge regions using high-resolution photoelectron spectroscopy at UVSOR-III BL7U. We used variable excitation photon energy from 7 to 40 eV and the photoelectron spectra were collected by an electron analyzer (A-1, MB-Scientific) with PBFDO sample at temperature from 10 to 298 K.

Figure 1 (a) and (b) show the valence band feature of PBFDO at 298 and 10 K compared to that of Au. It clearly demonstrates the metallic properties of PBFDO with metal-like Fermi edge. The valence feature at around 0.25 eV of PBFDO might be related to the filled LUMO, which results in a broad spectral feature crossing the Fermi edge as the lower part can be deconvoluted with metallic Fermi-Dirac function. Since there is short of theoretical analysis of the metallic properties of PBFDO, we may tentatively analyze the feature with the convolution of a gaussian valence peak at 0. 25 eV and metallic Fermi edge at 0 eV. Furthermore, Figure 1 (c) and (d) show the temperature dependent feature at 0 eV in PBDFO is very similar to that of Au metal. The broadening of the feature above the 0 eV monotonically increases with temperature. Based on our knowledge, the result is the first direct observation of the metallic Fermi feature in organic materials.

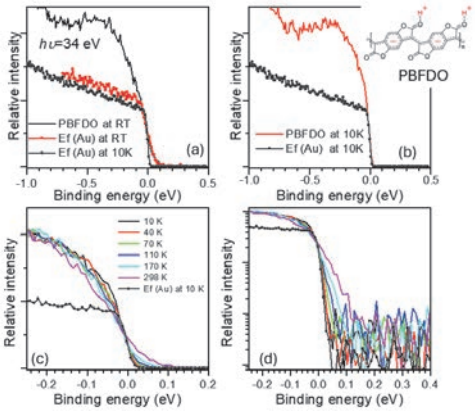

Fig. 1. Valence band feature of PBFDO at photon energy of 34 eV. (a,b) Comparison of Fermi edge feature of PBFDO and Au at 298 and 10 K. (c,d) Fermi edge feature of PBFDO as a function of temperature with linear (c) and logarithmic (d) intensity plots.

[1] A. Heeger, Angew. Chem. Int. Ed. **40** (2001) 2591.
[2] O. Bubnova *et al.,* Nat. Mater. **13** (2014) 190.
[3] A. Ruff *et al.,* Phys. Rev. Lett. **110** (2013) 216403.
[4] H. Tang *et al.*, Nature **611** (2022) 271.

BL7U

Coexistence of Ferromagnetism and Altermagnetism in MnTe Thin Films

R. Akiyama[1], T. T. Sasaki[2], M. Valvidares[3], T. Okauchi[4], K. Tanaka[5], S. Ichinokura[1,2], S. V. Ereemev[6], M. M. Otrokov[7], E. V. Chulkov[8], A. Hariki[4] and T. Hirahara[1]

[1]*Department of Physics, Institute of Science Tokyo, Tokyo 152-8551, Japan*
[2]*National Institute for Materials Science, Tsukuba 305-0047, Japan*
[3]*ALBA Synchrotron Light Source, E-08290 Cerdanyola del Valles, Spain*
[4]*Department of Physics and Electronics, Osaka Metropolitan University, Osaka 599-8531, Japan*
[5]*UVSOR III Synchrotron, Institute for Molecular Science, Okazaki 444-8585, Japan*
[6]*Institute of Strength Physics and Materials Science, Tomsk 634055, Russia*
[7]*Instituto de Nanociencia y Materiales de Aragón (INMA), Zaragoza 50009, Spain*
[8]*Donostia International Physics Center (DIPC), Basque Country, Spain*

Altermagnetic materials exhibit spin-compensated magnetic order like antiferromagnets while breaking time-reversal symmetry like ferromagnets [1]. MnTe, which has a NiAs-type structure, has been identified as an altermagnet with in-plane magnetic moments, as evidenced by nodal spin splitting observed in angle-resolved photoemission spectroscopy (ARPES) [2] and oscillatory x-ray magnetic circular dichroism (XMCD) signals [3]. In our previous study, we demonstrated that embedding 4 layers of MnTe into a topological insulator Bi_2Te_3 (BT) results in the formation of a $Mn_4Bi_2Te_7$/BT heterostructure, where the MnTe layers adjacent to the BT interface adopt a NaCl-type structure and the system exhibits out-of-plane ferromagnetism [4]. Building up on these findings, we consider embedding multilayer MnTe into the minimal unit of BT, a single quintuple layer (1QL- BT), which should allow the growth of MnTe thin films with surfaces and substrate interfaces terminated by Bi and Te atomic layers. However, the influence of such termination modifications on the altermagnetic properties of MnTe thin films remains unclear and requires investigation. Therefore in this study, we fabricated MnTe thin films terminated with Bi and Te atomic layers both at the surface and the interface to the Si substrate and compared their electronic structure with that of pure MnTe films directly grown on Si. Temperature and photon energy dependent *in situ* ARPES measurements were conducted at UVSOR BL-7U with p-polarized photons on and off the nodal plane. The energy and angular resolutions were 15 meV and 0.25°, respectively.

Scanning transmission electron microscopy (STEM) revealed that while these MnTe films terminated with Bi and Te predominantly exhibit the NiAs-type structure, NaCl-type stacking appears near the Si interface, resembling our previously reported $Mn_4Bi_2T_7$/BT heterostructure. XMCD measurements performed at BL29 BOREAS at ALBA confirmed the coexistence of altermagnetic and out-of-plane ferromagnetic signals, reproduced by ab inito calculations. This was also confirmed from ARPES measurements, as shown in Fig. 1. Upon cooling, the nodal splitting emerges in association with the altermagnetic transition (red arrow) at the nodal plane. Furthermore, an exchange splitting at the Γ point, likely induced by ferromagnetism, was also observed by further cooling as shown by the yellow arrow. In contrast, although the nodal splitting was observed for the pure MnTe film grown on Si, the exchange splitting was absent. This was consistent with the XMCD measurement. These findings indicate that the structural change at the interface cants the magnetic moment to the out-of-plane direction, resulting in the coexistence of altermagnetism and ferromagnetism in the MnTe films with Bi and Te termination.

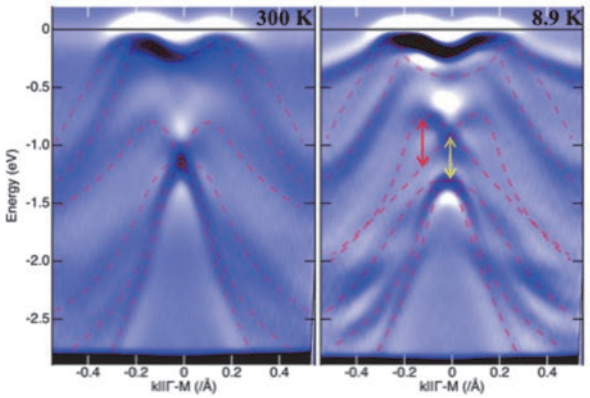

Fig. 1. Band structure of MnTe terminated with Bi and Te, measured along the Γ-M direction measured with hν = 19 eV. The left panel shows the paramagnetic state measured at T = 300 K and the right one shows the coexistence of altermagnetic and ferromagnetic states measured at T = 8.9 K. Red and yellow arrows indicate altermagnetic and ferromagnetic band splitting, respectively.

[1] L. Šmejkal *et al.*, Phys. Rev. X **12** (2022) 031042.
[2] S. Lee *et al.*, Phys. Rev. Lett. **132** (2024) 036702.
[3] A. Hariki *et al.*, Phys. Rev. Lett. **132** (2024) 176701.
[4] T. Hirahara *et al.*, Nat Commun. **11** (2020) 4821.

BL7U&5U

Changes in the Electronic Structure during the Charge-Density-Wave Transition Via the Well-Defined Temperature-Dependent Angle-Resolved Photoelectron Spectroscopy

S. Tanaka[1], K. Ueno[2] and K. Tanaka[3]
[1]*SANKEN, The University of Osaka, Mihogaoka 8-1, Ibaraki 567-0047, Japan*
[2]*Department of Chemistry, Graduate School of Science and Engineering, Saitama University, Saitama 338-8570, Japan*
[3]*UVSOR Synchrotron Facility, Institute for Molecular Science, Okazaki 444-8585, Japan*

The charge-density-wave (CDW) transition in titanium diselenide ($TiSe_2$) has attracted substantial interest due to its intriguing interplay between structural and electronic properties. Historically, X-ray diffraction studies have established a prominent structural transition near 202K [1], characterized predominantly by displacement of Ti atoms. More recently, advanced diffraction experiments revealed additional diffraction spots emerging at a lower temperature of approximately 165K, attributed primarily to the displacement of Se atoms which coincides with the peak-temperature observed in the resistivity change during the CDW transition [2]. Despite extensive structural investigations, detailed knowledge of how these distinct atomic rearrangements influence the electronic structure across the CDW transition remains incomplete.

In this study, we employ temperature-dependent angle-resolved photoelectron spectroscopy (ARPES) to investigate the electronic structure evolution of $TiSe_2$ across the CDW transition. The left panel of Fig. 1 presents ARPES spectra measured near the Γ point (top panel) and the L point (bottom panel) of $TiSe_2$, both below (left-hand side) and above (right-hand side) the CDW transition temperature. In the non-CDW phase (right-hand side), distinct features in the electronic states in $TiSe_2$ are Se4p-derived valence band and Ti3d conduction band located at the Γ and L points, respectively. The right panel of Fig. 1 displays the photoelectron intensity maps obtained along the momentum-space cuts indicated in the ARPES spectra, as a function of temperature. Our ARPES measurements reveal notable electronic signatures associated with the CDW transition including: (1) the folding of the Ti3d band from the Brillouin zone boundary (L point) toward near the zone center (Γ point), (2) the complementary folding of the Se4p band from near Γ toward the vicinity of the L point, and (3) a distinct binding energy shift of the Se4p band near the Fermi level.

Figure 2 illustrates the temperature dependence of the observed electronic signatures—specifically, the band folding intensity and energy shift—normalized such that values are set to 1 at 25 K and 0 at 200 K. The transition temperature for all the changes in the electronic structure is 165K, not the 202K. These observations indicate that the fundamental electronic reorganization in $TiSe_2$ is closely correlated with the lower-temperature structural transition involving Se atom displacement, rather than the higher-temperature transition predominantly involving Ti atom movements. Our findings clarify the relationship between electronic and structural transformations in $TiSe_2$ and underscore the critical role of Se atoms in driving the electronic properties of the CDW phase.

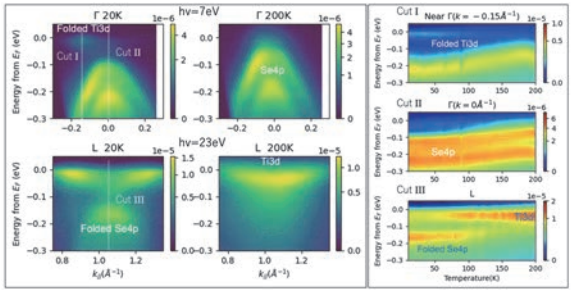

Fig. 1.
Left: the ARPES spectra near the Γ point (upper part) and L point (lower part) of $TiSe_2$ below the CDW temperature (left) and above (right).
Right: The photoelectron intensity map along the cut indicated in the ARPES spectra shown in the left panel as functions of the temperature.

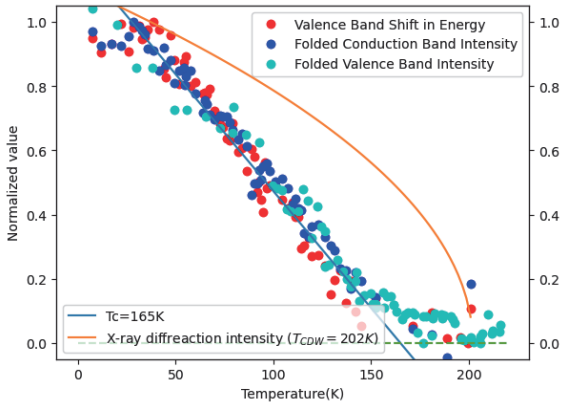

Fig. 2. Temperature dependence of the observed electronic signatures in $TiSe_2$, specifically the band folding intensity and binding energy shift, normalized to unity at 25 K and to zero at 200 K.

[1] F. J. Di Salvo, D. E. Moncton, and J. V. Waszczak, Phys. Rev. B **14** (1976) 4321.
[2] H. Ueda *et al.*, Phys. Rev. Res. **3** (2021) L022003.

BL7U

High-Resolution ARPES Study of Pure Electronic Nematicity in FeSe Thin Films on $LaAlO_3$

K. Nakayama[1], T. Kobayashi[2], F. Nabeshima[2], S. Souma[3,4], T. Takahashi[1], A. Maeda[2] and T. Sato[1,3,4,5,6]

[1]*Department of Physics, Tohoku University, Sendai 980-8578, Japan*
[2]*Department of Basic Science, the University of Tokyo, 3-8-1 Komaba, Meguro, Tokyo 153-8902, Japan*
[3]*Center for Spintronics Research Network, Tohoku University, Sendai 980-8577, Japan*
[4]*Advanced Institute for Materials Research (WPI-AIMR), Tohoku University, Sendai 980-8577, Japan*
[5]*International Center for Synchrotron Radiation Innovation Smart (SRIS), Tohoku University, Sendai 980-8577, Japan*
[6]*Mathematical Science Center for Co-creative Society (MathCCS), Tohoku University, Sendai 980-8578, Japan*

The iron-based superconductor FeSe is attracting considerable attention because it exhibits unique physical properties distinct from other iron-based superconductors, such as very strong coupling superconductivity in bulk samples and high-temperature superconductivity in monolayers. A particularly intriguing property is its electronic nematic state [Fig. 1(a)], in which the rotational symmetry of the electronic state is reduced from four-fold (C_4) to two-fold (C_2) [1]. While the electronic nematic state in other iron-based superconductors typically develops concurrently with antiferromagnetic order and a tetragonal-to-orthorhombic structural transition, the nematic state in FeSe is markedly different as it is not accompanied by antiferromagnetic ordering. In nearly all high-temperature superconductors discovered thus far, an antiferromagnetic phase exists adjacent to the superconducting phase, leading to the consideration of antiferromagnetic interactions as a primary candidate mechanism for high-temperature superconductivity. In this context, the results for FeSe are puzzling. Understanding the origin of the electronic nematic state is considered a crucial step towards the full understanding of the high-temperature superconductivity mechanism in iron-based superconductors.

As described above, the electronic nematic state in bulk FeSe is not accompanied by antiferromagnetic order. On the other hand, similar to other iron-based superconductors, it is known to undergo a tetragonal-to-orthorhombic structural transition. Therefore, the lattice also possesses C_2 symmetry. In a strict sense, this means the electronic state itself does not break the rotational symmetry independently of the lattice distortion. By contrast, we recently discovered that FeSe thin films grown on $LaAlO_3$ substrates exhibit a "pure" nematic state that emerges without accompanying antiferromagnetic order or even a structural phase transition [2]. Moreover, this pure nematic state coexists with superconductivity. Elucidating the complete picture of this novel electronic nematic state and its relationship to superconductivity is a critical research task.

In this work, we utilized high energy- and momentum-resolution capabilities at low-energy beamline BL7U to perform angle-resolved photoemission spectroscopy (ARPES) measurements on FeSe/$LaAlO_3$. High-quality FeSe/$LaAlO_3$ samples, prepared by pulsed laser deposition, were cleaved *in-situ* under ultrahigh vacuum to obtain clean surfaces suitable for ARPES. As shown in Fig. 1(b), we observed two hole-like branches around the M point of the Brillouin zone. This observation indicates the lifting of band degeneracy between the Fe 3d *xz* and *yz* orbitals, a hallmark of the electronic nematic state. We carefully investigated the evolution of these bands across the nematic transition. Furthermore, high-resolution measurements were performed at very low temperatures. From these comprehensive measurements, we obtained a detailed understanding of the pure nematic state.

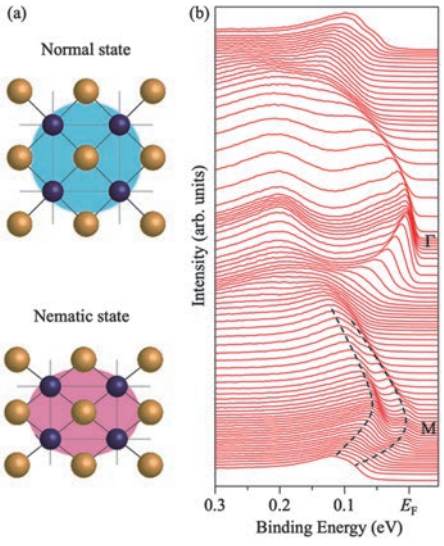

Fig. 1. (a) Schematic of crystal structure and electronic states in the normal state (top) and nematic state (bottom) in bulk FeSe [2]. (b) ARPES spectra along the ΓM high-symmetry line measured in the pure electronic nematic state of FeSe/$LaAlO_3$.

[1] K. Nakayama *et al.*, Phys. Rev. Lett. **113** (2014) 237001.
[2] Y. Kubota *et al.*, Phys. Rev. B **108** (2023) L100501.

BL7U

Band Dispersion of the Topological Nodal-Line Semimetal KAlGe

T. Ishida[1], S. Huh[1], T. Ikenobe[1], T. Yamada[2], J. Junhyeok[1], A. Mine[1], S. Makita[3], K. Tanaka[3], Z. Hiroi[1] and T. Kondo[1]

[1]*Institute for Solid State Physics, The University of Tokyo, Kashiwa, Chiba 277-8581, Japan*
[2]*IMRAM, Tohoku University, Sendai 980-0812, Japan*
[3]*UVSOR Facility, Institute for Molecular Science, Okazaki, Aichi 444-8585, Japan*

The compounds NaAlSi, NaAlGe, and KAlGe are part of a family of topological nodal-line semimetals. These materials share nearly identical crystal and electronic structures according to first-principles calculations [1]. However, they display strikingly different physical properties: NaAlSi becomes superconducting below ~7 K, NaAlGe exhibits a pseudogap-like behavior near 100 K, while KAlGe undergoes a metal-to-metal transition at 89 K. This divergence in physical phenomena, despite similar electronic band topology, raises important questions about the underlying mechanisms. In NaAlSi, recent studies suggest that many-body interactions significantly enhance the effective mass of the Fermi surface, contributing to its superconductivity [2]. ARPES measurements have confirmed the existence of a flat band near or just below the Fermi level, which is interpreted as a manifestation of mass enhancement [3]. Furthermore, two topological nodal lines are clearly resolved. To understand the unique behavior of KAlGe, we aim to clarify its band dispersion, especially the position of the flat band, through angle-resolved photoemission spectroscopy (ARPES). Despite theoretical predictions, no experimental band structures for KAlGe have been reported to date, making our study the first direct observation. Single crystals of KAlGe were synthesized using a potassium–indium flux method. Owing to their air sensitivity, all handling and sample preparation were conducted in an argon-filled glovebox. The samples were cleaved *in-situ* under ultrahigh vacuum conditions (4.0×10^{-9} Pa) immediately prior to measurement to expose pristine surfaces. ARPES experiments were performed at 120 K using 17 eV photons at the UVSOR BL7U beamline. Both linear horizontal (LH) and vertical (LV) polarizations were used to probe orbital character.

Figure. 1 consents constant-energy mappings of KAlGe measured with 17 eV LH-polarized light. The overall shape and symmetry closely resemble those of NaAlSi, indicating that the bulk electronic structure is largely conserved within this family. Figure 2 shows the band dispersions along the Γ–X direction. The left and right panels correspond to LH and LV polarization, respectively. Under LH light, we observe features dominated by the Ge $4p_x$ orbital (highlighted in yellow), whereas LV polarization enhances the Ge $4p_y$ orbital (blue). The Al 3s orbital is not clearly observed under either polarization, likely due to matrix element suppression. Most notably, unlike NaAlSi, the flat band is absent below the Fermi energy in KAlGe. This suggests a crucial difference in many-body renormalization or hybridization strength. We propose that the elevated position of the flat band in KAlGe may suppress the density of states at the Fermi level, thereby inhibiting superconductivity while allowing alternative phenomena such as the observed metal-to-metal transition. The polarization dependence also supports orbital selectivity in KAlGe, possibly tied to the directionality of nodal-line dispersion and spin-orbit coupling. Further photon energy- dependent measurements are planned to confirm the three-dimensional character of the observed bands.

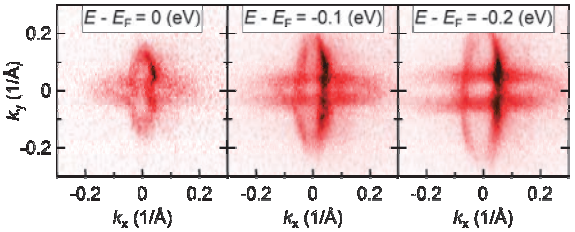

Fig. 1. Constant energy mapping of KAlGe at 120 K with 17 eV LH polarized light.

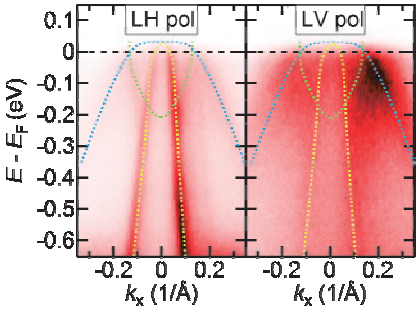

Fig. 2. Electronic structure of KAlGe at 120 K with 17 eV light in Γ-X.

[1] T. Ikenobe, *et al*., Chem. Mater. **37**(1) (2024) 189.
[2] S. Uji, *et al*, Phys Rev B **105** (2022) 235103.
[3] C. Song, *et al*., Phys Rev B **105** (2022) L161104.

III-2

BL7U

High-Resolution ARPES Study of Topological Superconductor Candidate $PtBi_2$

Y. Morita[1], K. Nakayama[1], T. Kato[2], S. Souma[2,3], S. Masaki[4], T. Ikushima[4], Y. Moriyasu[4], K. Hagiwara[5], F. Matsui[5], K. Tanaka[5,6], T. Takahashi[1], K. Kudo[4] and T. Sato[1,2,3,7,8]

[1]*Department of Physics, Tohoku University, Sendai 980-8578, Japan*
[2]*Advanced Institute for Materials Research (WPI-AIMR), Tohoku University, Sendai 980-8577, Japan*
[3]*Center for Science and Innovation in Spintronics (CSIS), Tohoku University, Sendai 980-8577, Japan*
[4]*Department of Physics, Graduate School of Science, The University of Osaka, Toyonaka 560-0043, Japan*
[5]*UVSOR Synchrotron Facility, Institute for Molecular Science, Okazaki 444-8585, Japan*
[6]*School of Physical Sciences, The Graduate University for Advanced Studies (SOKENDAI), Okazaki 444-8585, Japan*
[7]*International Center for Synchrotron Radiation Innov1ation Smart (SRIS), Tohoku University, Sendai 980-8577, Japan*
[8]*Mathematical Science Center for Co-creative Society (MathCCS), Tohoku University, Sendai 980-8578, Japan*

Following the discovery of topological insulators, the exploration for new topological materials is actively progressing. A prime example is the Dirac semimetal, which features a Dirac-cone-type band dispersion where the bulk conduction and valence bands touch at discrete points in three-dimensional Brillouin zone. These materials hold promise for applications in next-generation ultra-high-speed electronics and spintronics. Furthermore, among topological semimetals, Weyl semimetals host spin-polarized Dirac cones (Weyl cones) in their bulk band structure. Weyl semimetals are realized in systems where spatial inversion or time-reversal symmetry is broken. Numerous quantum phenomena, such as the anomalous Hall effect and the chiral anomaly, are predicted for Weyl semimetals, and their experimental verification is actively underway. In recent years, aiming to realize even more exotic topological phases, the exploration of materials that integrate superconductivity with Dirac or Weyl semimetal states has become a key research objective. Introducing superconductivity is anticipated to facilitate the formation of unconventional Cooper pairs, potentially leading to topological superconductivity and Majorana fermions.

Here, we focus on $PtBi_2$ [Fig. 1(a)], a transition metal dichalcogenide with broken spatial inversion symmetry. This material is a Weyl semimetal candidate and exhibits bulk superconductivity below 0.6 K. Moreover, a recent report suggests potential surface superconductivity with a significantly higher transition temperature above 10 K [1]. These combined Weyl semimetallic and superconducting characteristics make $PtBi_2$ a promising platform for exploring topological superconductivity. However, key aspects of its electronic structure relevant to topological superconductivity, such as bulk Weyl cones, require further investigation.

Using bulk-sensitive low-energy photons at BL7U, we mapped the three-dimensional bulk electronic structure of $PtBi_2$. Our results shown in Fig. 1(b) reveal signatures of spin-split bulk bands, recognized from Rasha-like band dispersion observed around the M point. Such spin splitting, likely originating from the broken inversion symmetry, is a prerequisite for the predicted Weyl semimetal phase. To further investigate this phase, we performed high-resolution measurements to directly observe the Weyl cones near the Fermi level.

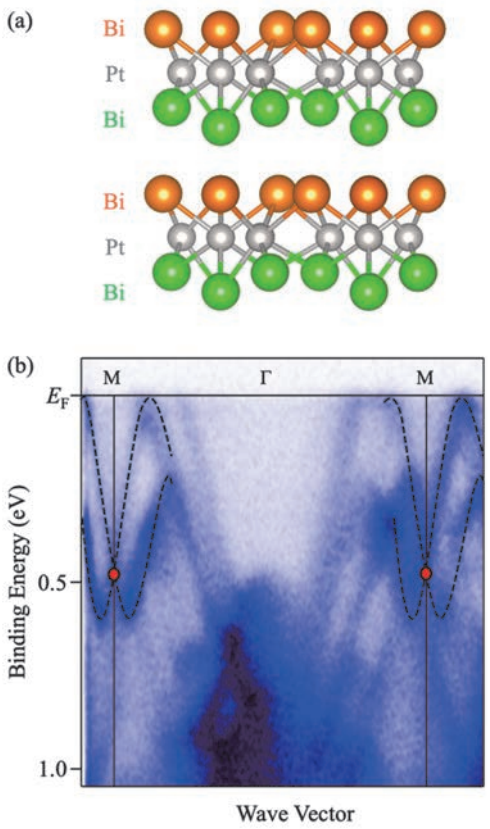

Fig. 1. (a) Crystal structure of $PtBi_2$. (b) Plot of ARPES intensity measured in the normal state along the ΓM high-symmetry line.

[1] A. Kuibarov *et al.*, Nature **626** (2024) 294.

BL7U

Probing Hole Doping Effects in Ti-Substituted Ta_2NiSe_5 Investigated by Angle-Resolved Photoemission Spectroscopy

J. Han[1], K. Aido[1], S. Tsuchida[2], Y. Hirose[2], R. Settai[2], S. Makita[3], K. Tanaka[3] and T. Kondo[1]
[1]*ISSP, University of Tokyo, Kashiwa, Chiba 277-8581, Japan*
[2]*Department of Physics, Niigata University, Niigata 950-2181, Japan*
[3]*UVSOR Facility, Institute for Molecular Science, Okazaki, Aichi 444-8585, Japan*

Ta_2NiSe_5 has emerged as one of the most prominent candidates for excitonic insulator systems. With a direct band gap, it undergoes an insulating transition accompanied solely by a $q = 0$ structural distortion at T_s = 329 K, without charge density wave (CDW) formation [1]. A central issue in this field is whether the transition is primarily driven by excitonic condensation or by lattice instability. Since exciton formation originates from the Coulomb attraction between electrons and holes, tuning the screening strength through carrier doping could facilitate a disentangled investigation of the respective roles played by electronic and structural degrees of freedom.

To systematically explore the effects of carrier doping, we investigated the electronic structure of Ti-substituted Ta_2NiSe_5, where Ti atoms replace Ta sites, introducing effective hole doping due to the difference in their valence electron configurations. Single crystals of pristine and Ti-substituted Ta_2NiSe_5 were synthesized by the chemical vapor transport method. The samples were cleaved *in-situ* to obtain clean surfaces for measurements. Angle-resolved photoemission spectroscopy (ARPES) measurements were performed at BL7U of UVSOR with a photon energy of 18 eV. All data were collected at a sample temperature of 83 K (below T_s). To distinguish the orbital characters associated with Ta, Ni, and Se atoms, both linear vertical (LV) and linear horizontal (LH) polarizations were employed during the measurements [2].

Figure 1 compares the band structures along the Γ-X direction for pristine and Ti-substituted Ta_2NiSe_5. Under LV polarization [Figs. 1(a) and 1(b)], bands primarily derived from Ta 5*d* orbitals are selectively enhanced, while LH polarization emphasizes the Ni 3*d*-derived bands [Figs. 1(c) and 1(d)]. In the pristine sample [Figs. 1(a) and 1(c)], the characteristic flat top of the valence band, associated with the excitonic insulating state, appears near a binding energy of approximately 170 meV. Upon Ti substitution [Figs. 1(b) and 1(d)], the overall band structure, which includes the characteristic flat band, shifts toward lower binding energies without significant deformation compared to the pristine one. This implies that the level of Ti substitution may not yet be sufficient to induce a complete insulator-to-semimetal transition.

Assuming that carrier doping suppresses exciton condensation, the upward shift of the flat-top valence band to approximately 60 meV can be regarded as an indication of gap narrowing. As highlighted by the black arrows in Figs. 1(b) and 1(d), only the spectral weight near the Fermi level (E_F) is depleted, which may suggest the emergence of a pseudogap. With a slightly higher level of Ti substitution, the bands may begin to overlap, potentially leading to a semimetallic transition. Unlike previous approaches based on potassium deposition [3], our substitution-based strategy avoids interpretational ambiguities arising from the Stark effect, thereby offering a cleaner platform to disentangle the respective roles of electronic and lattice degrees of freedom in the excitonic insulating state.

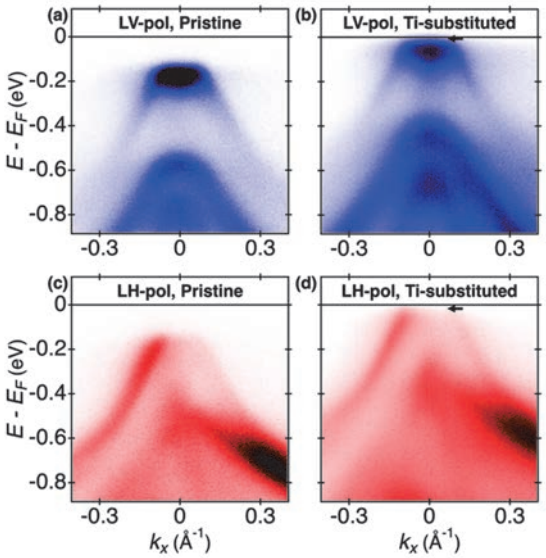

Fig. 1. Polarization-dependent ARPES spectra of pristine (a,c) and Ti-substituted (b,d) Ta_2NiSe_5 along the Γ-X direction, measured with LV (a,b) and LH (c,d) polarizations. Black arrows indicate spectral weight suppression near E_F .

[1] Y. Wakisaka *et al*., Phys. Rev. Lett. **103** (2009) 026402.
[2] T. Kaneko *et al*., Phys. Rev. B **87** (2013) 035121.
[3] X. Chen *et al*., Phys. Rev. Res. **5**,(2023) 043089.

BL7U

Observation of Electronic Structure of Organic Mott Insulator β'-(BEDT-TTF)$_2$ICl$_2$ by Angle-Resolved Photoelectron Spectroscopy

R. Nakazawa[1], K. Fukutani[1], Y. Ishida[2], S. Makita[3], K. Tanaka[3], T. Kobayashi[4], H. Taniguchi[4] and S. Kera[1,2,3]

[1]*Department of Photo-Molecular Science, Institute for Molecular Science, Okazaki 444-8585, Japan*
[2]*Faculty of Engineering, Chiba University, Chiba 263-8522, Japan*
[3]*UVSOR Synchrotron Facility, Institute for Molecular Science, Okazaki 444-8585, Japan*
[4]*Faculty of Science, Saitama University, Saitama 338-8570, Japan*

Organic materials have the potential to promote the sustainable development of science and technology due to their flexibility and high environmental compatibility. Among them, strongly correlated organic molecular crystals exhibit a variety of quantum phases, such as superconductivity, spin liquid state, Mott insulating phase, and topological phase [1, 2].

(BEDT-TTF)$_2$X belongs to the strongly correlated organic molecular crystals and is a charge-transfer complex. Here, X means anion. Due to the electron transfer of the BEDT-TTF molecule to X, the valence band described from the highest occupied molecular orbital (HOMO) offers a half-filled or 1/4 filled. Whether the system is a metallic phase or an insulating phase depends on the microscopic electronic structure with Coulomb interaction energy. In the case of the half-filled band for a dimer state and large Coulomb interaction energy, the valence band from the anti-bonding HOMO state splits into upper and lower Hubbard bands, leading to an insulating phase which is called Mott insulator.

While the origins of the Mott insulator phase are largely encoded in the electronic structures as mentioned above, direct experimental data on the momentum-resolved electronic structure is missing. In the case of a Mott insulator, β'-(BEDT-TTF)$_2$ICl$_2$ [3, 4], electrical measurements confirm that it is an insulating phase at ambient pressure [1]. On the other hand, the band obtained by theoretical calculations crosses the Fermi level because they do not correctly account for the Coulomb interaction [5], and the true picture of electronic structure of this material is not unclear. To understand the many-body nature of β'-(BEDT-TTF)$_2$ICl$_2$, such as whether this material has the electronic states as a metallic phase or an insulating phase, first it is important to directly observe the momentum-resolved electronic structures which previous studies lack.

In this study, we observed the valence band electronic structure of β'-(BEDT-TTF)$_2$ICl$_2$ using angle-resolved photoelectron spectroscopy (ARPES) at BL7U in UVSOR.

Figure 1 shows the valence band structure observed using excitation energy of $h\nu$ = 40 eV at T = 150 K. Fig.1(a) shows the photoemission intensity plot along the short crystal axis (c-axis), and Fig. 1(b) is the corresponding second derivative plot. A dispersive band with the width of ~0.14 eV is observed at the binding energy (E_b) of ~0.7 eV. Since the observed band periodicity corresponds to the periodicity of Brillouin zone, we judged that we have successfully observed itinerant electrons in this material. In addition, the band with almost no dispersion was observed at the E_b of ~0.4 eV. These bands at the E_b of ~0.4 and ~0.7 eV are ascribed to the lower Hubbard and the bonding band, respectively. Moreover, we have successfully observed the photoelectrons along other high-symmetric momentum directions to reveal the details of the electronic structures.

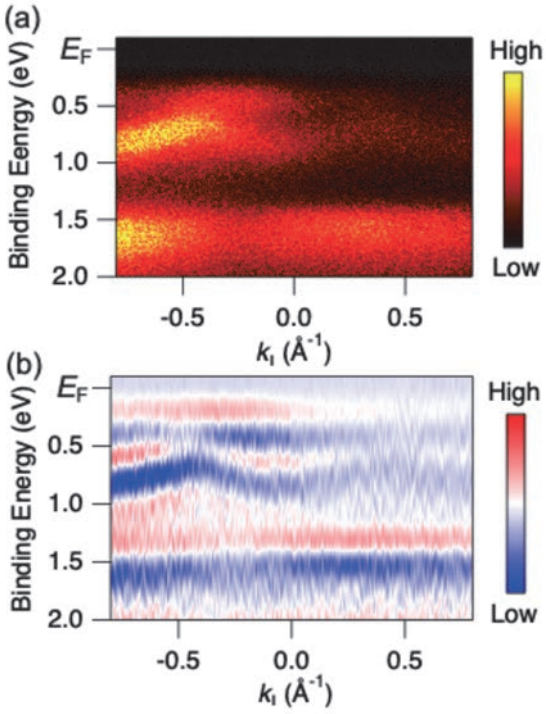

Fig. 1. (a) Photoemission intensity plot, and (b) the corresponding second derivative plot of β'-(BEDT-TTF)$_2$ICl$_2$ crystal observed at $h\nu$= 40 eV, T = 150 K.

[1] K. Kanoda, J. Phys. Soc. Jpn. **75** (2006) 051007.
[2] T. Nomoto *et al.*, Nat. Commun. **14** (2023) 2130.
[3] T. J. Emge, *et al.*, J. Am. Chem. Soc. **108** (1986) 695.
[4] H. Kobayashi, *et al.*, Chem. Lett. **15** (1986) 89.
[5] T. Koretsune, C. Hotta, Phys. Rev. B **89** (2014) 045102.

Angle-Resolved Photoemission Study of Layered MAB Phase Compounds MoAlB

T. Ito[1,2], K. Kawano[1], N. Yuanzhi[1], M. Nakatake[3], K. Tanaka[4,5], A. Sharma[6], H. Pazniak[6] and T. Ouisse[6]

[1]*Graduate School of Engineering, Nagoya University, Nagoya 464-8603, Japan*
[2]*Synchrotron radiation Research center, Nagoya University, Nagoya 464-8603, Japan*
[3]*Aichi Synchrotron Radiation Center, Seto 489-0965, Japan*
[4]*UVSOR Facility, Institute for Molecular Science, Okazaki 444-8585, Japan*
[5]*The Graduate University for Advanced Studies, Okazaki 444-8585, Japan*
[6]*Grenoble Alpes, CNRS, Grenoble INP, LMGP, F-38000 Grenoble, France*

MAB phase compounds are layered compounds formed by combining transition metals M and III-A (IV-A) group elements A and B, and have a layered crystal structure in which a strong MB layer and two A layers are stacked in the b-axis direction [1]. In this system, it is expected that the atomic layer system MBenes formed only from MX layers will be obtained by removing the A atoms by HF treatment or exfoliation. Therefore, this system has attracted attention in recent years as a new atomic layer system that can replace graphene [2]. Among boron compounds, MoAlB is known to be an excellent system, especially in terms of applications, due to its relatively good processability, high temperature oxidation resistance, high thermal conductivity, and high electrical conductivity. Furthermore, the results of DFT calculations [3] predict a three-dimensional Dirac semimetal nature of MoAlB. In this study, we have performed angle-resolved photoemission spectroscopy (ARPES) on MAB phase compound MoAlB to directly investigate the electronic structure of this system.

ARPES measurements were performed at the UVSOR-III BL7U. Inter-plane ARPES data were acquired with using $h\nu$ = 11 - 30 eV at T = 30 K. Single crystals were cleaved in situ along (010) plane.

Figure 1(a) shows the obtained Fermi surface (FS) image on the ΓYZT plane . It has been found that the electronic structure around ΓZ line formed by two hole-like FSs with quasi-two-dimensional character, which are qualitatively reproduced by density functional theory (DFT) calculations (not shown). On the other hand, we have found three dimensional FS around Z point and $k_y \sim$ -0.5 Å^{-1} around ΓY line. To elucidate three-dimensional electronic structure of MoAlB, we indicate inter-plane ARPES image along ΓZ line in Fig. 1(b). The inner potential V_0 is estimated to be 27 eV based on the symmetry of the dispersive features. From the comparison between ARPES and DFT calculation, narrow parabolic dispersions around 0.5 and 2.7 eV seem to show qualitative agreement. However, a sharp, flat pocket symmetrically observed around the Z point on the present ARPES is not predicted by the DFT calculations. Although the origin of this discrepancy remains unclear, it is plausible that the formation of the heavy electron surface is associated with a chemical potential shift of approximately 100 meV. To pursue the relation between anomalous FS and the thermodynamic properties of MoAlB, further studies are intended.

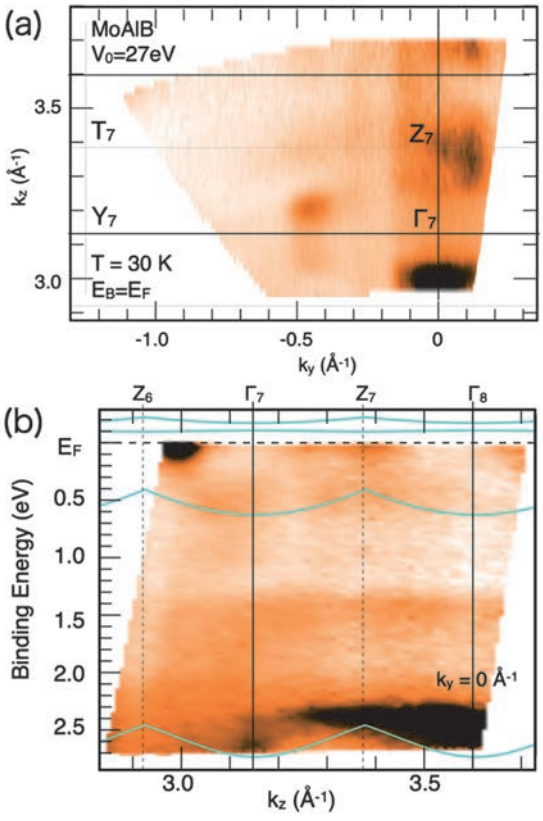

Fig. 1. (a) Fermi surface along ΓYZT plane of MoAlB obtained by inter-plane ARPES measurements. (b) Inter-plane ARPES image along ΓZ line. Solid lines are DFT calculation along ΓZ line.

[1] Y. Huang *et al*., Small **18** (2022) 2104460.
[2] X. Zhu *et al*., Nature Commun. **12** (2021) 4080.
[3] Y. Huang *et al*., Materials Today Physics **33**(2023) 101060.

BL7U

Exploration of Electronic Band Structure and Topological Surface States in Ni-Doped PdSeTe

Y. Kumar[2], S. Ideta[1,2] and K. Shimada[1,2]

[1]*Graduate School of Advanced Science and Engineering, Hiroshima University, Hiroshima 739-0046, Japan.*
[2]*Hiroshima Research Institute for Synchrotron Radiation Science (HiSOR), Hiroshima University, Hiroshima 739-0046, Japan.*

In recent years, exploring the electronic structures of topological insulators and topological semimetals has become a central focus in condensed matter physics. Among these, Dirac and Weyl semimetals have attracted significant attention, particularly in the realm of spintronics, due to their unique and enhanced physical properties [1, 2]. Layered transition-metal dichalcogenides (TMDCs) with the chemical formula AB_2 (where A is a transition metal and B is a chalcogen) have been the subject of extensive research due to their diverse range of physical properties, including superconductivity and the emergence of charge density waves (CDWs).

Recently, we have reported the existence of topological surface states and enhancement of superconducting transition temperature in 1T-PdSeTe [3], which is the sister compound of $PdTe_2$ by replacing 50% of Te atoms with Se, trying to break the inversion symmetry to create a Weyl semimetal. We explored the surface and bulk electronic structures of the superconducting type-II Dirac semimetal 1T-PdSeTe, which exhibits a superconducting transition temperature (T_C = 3.2 K) nearly twice that of its counterpart 1T-PdTe$_2$ (T_C = 1.6 K). Angle-resolved photoemission spectroscopy (ARPES) and density functional theory (DFT) analyses revealed topological surface states and electronic band structures closely resembling those of 1T-PdTe$_2$. These findings suggest that the CdI_2-type lattice symmetry plays a dominant role in dictating the band dispersion, largely unaffected by atomic-scale disorder in the chalcogen layers. To the best of our knowledge, we were the first to demonstrate that the PdSeTe superconductor hosts topological surface states.

In order to break the time reversal symmetry in this material, we have tried to dope a magnetic impurity (Ni) at the Pd-site. We have successfully grown the $Ni_xPd_{1-x}SeTe$ single crystals. We have measured the electronic band structure using ARPES at BL7U at UVSOR. The objective of this study was to carry out ARPES measurements on Ni-doped PdSeTe samples to elucidate their electronic band structure. Particular emphasis was placed on analyzing the band dispersion and Fermi surface with the goal of identifying signatures of topological surface states and Fermi arcs. We have prepared $Ni_xPd_{1-x}SeTe$ samples and aligned them in a high-symmetry direction using the Laue diffraction (XRD) available at the UVSOR-III synchrotron facility to accurately measure the band dispersion in the high-symmetry direction.

We have cleaved three samples of $Ni_xPd_{1-x}SeTe$ to obtain a clean surface; the cleave was very good, resulting in the sharp band dispersion. We have performed the ARPES experiment and mapped the Fermi surface at photon energy 25 eV as shown in Fig. 1. Also, I have measured high symmetry cuts in the Γ-M direction to investigate the electronic band structure with both *s*- and *p*-polarizations. I have performed the photon energy-dependent measurement from 9 eV to 25 eV to observe the k_z dependence. We have also optimized the beam slit to improve the data quality and resolution. Detailed records of experimental procedures, sample characteristics, and measurement results were maintained during the experiment. We have to do further measurements to complete the data set.

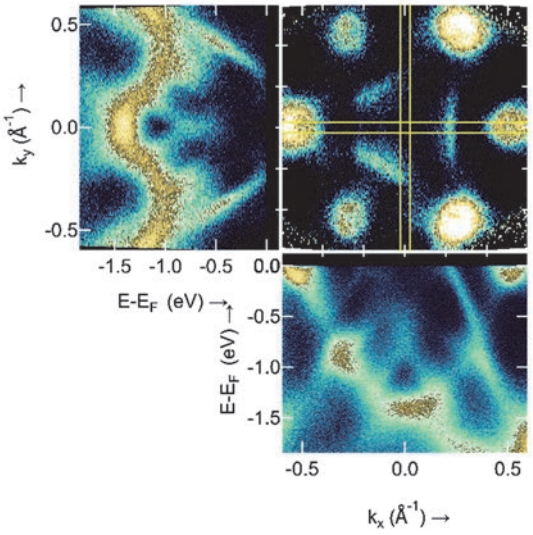

Fig. 1. Fermi Surface of $Ni_xPd_{1-x}SeTe$ single crystal at 25 eV alongside band dispersion in the K-Γ-K and M-Γ-M directions.

[1] N. P. Armitage, E. J. Mele, A. Vishwanath, Rev. Mod. Phys. **90** (2018) 015001.
[2] A. A. Burkov, Nat. Mater. **15** (2016) 1145.
[3] Y. Kumar, K. Shimada *et al*, Phys. Rev. Res. **7** (2025) 013174.

Role of Orbital-Selective Mott Phase on Topological Properties in Iron Chalcogenide Superconductors

Y. Kim[1], J. Yoo[1], S. Kim[1] and C. Kim[1]
[1]*Department of Physics and Astronomy, Seoul National University, Seoul 08826, South Korea*

Orbital-selective Mott phase (OSMP), where one band becomes effectively localized while other bands remain metallic, emerges in correlated multiorbital systems. In electronic structures, the OSMP is characterized by a loss of spectral weight and broadening of the associated band at high temperatures [1]. This phenomenon has attracted much attention since its ubiquity; many strongly correlated multiorbital systems exhibit OSMP. Despite such interests to OSMP, research on its relation to practical physical properties remains elusive.

Here, we investigate the relationship between OSMP and non-trivial topology in $FeTe_{1-x}Se_x$ (FTS), iron chalcogenide superconductors. FTS exhibit non-trivial topology as well as unconventional superconductivity. The non-trivial topology arises from the band inversion of the odd-parity p_z and d_{xz} bands along the Γ – Z line [2]. This in turn suggest that to study the impact of the OSMP on the topological properties of FTS, it is necessary to investigate the electronic structures of FTS along the Γ – Z line.

In ARPES measurements, two aspects should be considered for the measurements; i) as the band of interest is pz band, photon energy should be lower than 20 eV considering photoionization cross section ii) photon energy should be tunable for the k_z-dependent measurements. UVSOR Beamline 7U satisfies the aforementioned conditions [3]. Here, we report successful measurement results of the electronic structures of FTS along the Γ – Z line as a function of Se/Te ratio and temperature in BL 7U.

Shown in Figs. 1**a-d** are electronic structures of FTS along the Γ – Z line with selenium contents of x = 0.04, 0.09, 0.19, and 0.31, respectively. They all show a dispersive band, which can be attributed to the odd-parity p_z band. To track the evolution of the p_z band as a function of doping, the top and bottom positions of the band at the Γ and Z points, respectively, are extracted from a two-dimensional fitting as shown in Fig. 1**e**. The p_z band overall moves towards lower energy for lower Se contents. The notable point of the doping-dependent evolution is that the band at the top of the p_z band at the Γ point goes below the Fermi level at x = 0.04. If the p_z band goes below the d_{xz} band which is near the Fermi level, this makes the inversion parities of the Γ and Z both odd, resulting in trivial topology. This suggests that topological phase transition occurs between x = 0.04 and 0.09, resulting in trivial topology at x = 0.04.

Figures 1**f**–**i** show temperature-dependent ARPES results for the sample with x=0.19 measured at temperatures of 30 K, 50 K, 90 K, and 175 K, respectively. Unlike the doping-dependent behavior, the position of the odd-parity band does not change with temperature.

In summary, we have successfully measured the odd-parity band in FTS, providing insights into its topology. These results may shed light on the role of OSMP in determining the system's topological properties.

[1] M. Yi *et al.*, npj Quantum Mater. **2** (2017) 57.
[2] P. Zhang *et al.*, Science **360** (2018) 6385.
[3] Y. Kim *et al.*, Nat. Commun. **14** (2023) 4145.

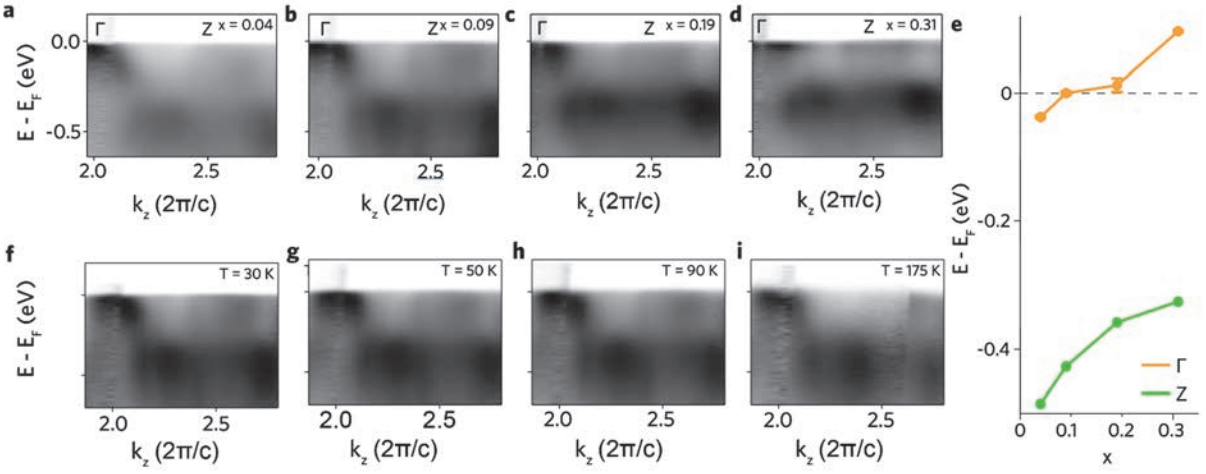

Fig. 1. **a-d** Band dispersion along Γ − Z, with selenium contents of x = 0.04, 0.09, 0.19, and 0.31, respectively. e Position of the p_z band at the Γ and Z points. **f-i** Band dispersion along Γ − Z, with temperatures of 30 K, 50 K, 90 K and 175 K, respectively.

Electronic Structure Study of Topological Materials $Ge_2Bi_2Te_5$ and $Ge_3Bi_2Te_6$

Y. Dai[1], X. M. Ma[1] and C. Liu[1]
[1]*Southern University of Science and Technology (SUSTech), Shenzhen, Guangdong 518055, China*

The $MnBi_2Te_4(Bi_2Te_3)_n$ compounds, with $MnBi_2Te_4$ being a prototypical member, have been established as model systems of intrinsic magnetic topological insulators [1-3]. The characteristic van der Waals structure of $MnBi_2Te_4$ comprises alternating Te-Bi-Te-Mn-Te-Bi-Te layers with single Mn layers per unit cell, supporting antiferromagnetic (AFM) ordering below 24 K and manifesting intricate magneto-topological coupling [4, 5]. However, a fundamental constraint arises from the limited magnetic layer density: the single-Mn-layer configuration leads to weak interlayer magnetic coupling and suppresses Neel temperatures, hindering potential applications.

Recent theoretical works propose that structural engineering through magnetic layer stacking – as exemplified in $Mn_2Bi_2Te_5$ and $Mn_3Bi_2Te_6$ derivatives – could enhance magnetic ordering temperatures [6, 7]. On one hand, $Mn_2Bi_2Te_5$ has been predicted to host a *dynamic axion insulator* state, offering an unprecedented platform for exploring topological electromagnetic responses [6]. On the other hand, first-principles calculations reveal a magnetic-order-dependent topological phase transition in $Mn_3Bi_2Te_6$, with the AFM configuration remaining topologically trivial while the ferromagnetic (FM) ordering induces nontrivial topology [7]. Despite these compelling predictions, experimental verification remains elusive due to formidable single-crystal growth challenges.

To circumvent the synthesis bottleneck, we adopt a chemical substitution strategy leveraging the structural stability of isostructural germanium analogs $Ge_2Bi_2Te_5$ and $Ge_3Bi_2Te_6$ [8, 9]. Through progressive substitution of Ge with Mn in $(Ge_{1-x}Mn_xTe)_mBi_2Te_3$ (m = 2, 3), we aim to engineering systems combining robust magnetic ordering with topological functionality.

Our experimental investigation combines angle-resolved photoemission spectroscopy (ARPES) measurements at UVSOR BL7U with systematic Mn doping. Initial characterization of parent compounds $Ge_2Bi_2Te_5$ (Fig. 1a) and $Ge_3Bi_2Te_6$ (Fig. 2a) established baseline electronic structures. Subsequent doping studies focus on nominal Mn concentration of 20% and 30% in $(Ge_{1-x}Mn_x)_2Bi_2Te_5$, and 30% in $(Ge_{1-x}Mn_x)_3Bi_2Te_6$.

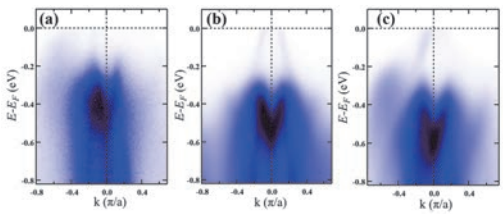

Fig. 1. Band evolution on $(Ge_{1-x}Mn_x)_2Bi_2Te_5$ with different nominal Mn doping levels x = 0 (a), x = 0.2 (b) and x = 0.3 (c) ($h\nu$ = 20 eV). The measurement direction is Γ-M for (a) and (c), and Γ-K for (b). As x increases, the Fermi level moves upward.

ARPES data reveal progressive Fermi level upshifting with increasing Mn content, indicative of n-type dosage. The $(Ge_{1-x}Mn_x)_3Bi_2Te_6$ system manifests electronic features suggestive of hole-doped analogs to its m = 2 counterpart. While both systems preserve threefold rotational symmetry in constant-energy contours (Fig. 3d), subtle differences in their band dispersion await theoretical interpretation.

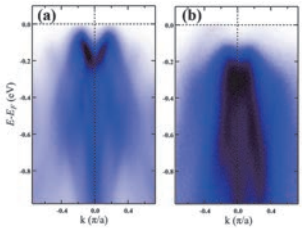

Fig. 2. Band evolution on $(Ge_{1-x}Mn_x)_3Bi_2Te_6$ with different nominal Mn doping levels x = 0 (a) and x = 0.2 (b) ($h\nu$ = 20 eV). The measurement direction is Γ-K for (a) and Γ-M for (b). As x increases, the Fermi level moves upward.

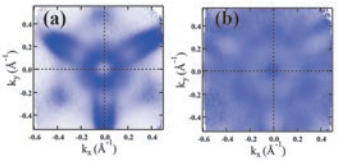

Fig. 3. ARPES constant-energy contour of $(Ge_{0.8}Mn_{0.2})_2Bi_2Te_5$ with $h\nu$ = 21 eV. The binding energy of each penal is 0.25 eV (a) and 1.35 eV (b).

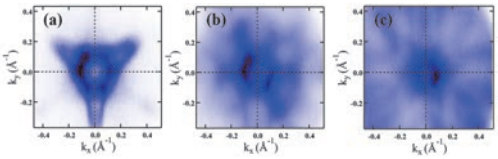

Fig. 4. ARPES constant-energy contour of $Ge_3Bi_2Te_6$ with with $h\nu$ = 19 eV. The binding energy of each penal is 0.05 eV (a), 0.35 eV (b) and 1.45 eV (c).

[1] D. Zhang *et al*., Phys. Rev. Lett. **122** (2019) 206401.
[2] Klimovskikh *et al*., npj Quantum Mater. **5** (2020) 54.
[3] H. Deng *et al*., Nat. Phys. **17** (2021) 36.
[4] J. Zhang *et al*., Chin. Phys. Lett. **37** (2020) 077304.
[5] A. Gao *et al*., Nature **595** (2021) 521.
[6] J. Zhang *et al*., Chin. Phys. Lett. **37** (2020) 077304.
[7] W. Wu *et al*., J. Phys.: Condens. Matter **36** (2024) 125701.
[8] Matsunaga *et al*., Acta Cryst. B **63** (2007) 346.
[9] L. E. Shelimova *et al*., Inorganic Materials **36** (2000) 235.

BL7U

Electronic State Analysis of Bcc-Cu Thin Film on FeCo/MgO(100)

S. Takezawa[1,2] and N. Nagamura[1,2,3]

[1]*Graduate School of Advanced Engineering, Tokyo University of Science, Tokyo 125-8585, Japan*
[2]*Center for Basic Research on Materials, National Institute for Materials Science, Tsukuba 305-0003, Japan*
[3]*Research Institute of Electrical Communication, Tohoku University, Sendai 980-0812, Japan*

Copper typically crystallizes in a face-centered cubic (fcc) structure as its most stable phase. However, in nanocrystalline systems or certain ultrathin films, it can adopt a metastable body-centered cubic (bcc) structure[1,2]. Notably, bcc-Cu/FeCo multilayers have been reported to exhibit high magnetoresistance (MR) ratios in three-layer giant magnetoresistance (GMR) devices[3]. This enhancement in MR ratio is strongly influenced by modulation of the electronic states at the Cu/FeCo interface, which arises from the formation of the metastable Cu phase. Nevertheless, there have been no experimental reports directly observing the electronic structure of bcc-Cu and its thickness-dependent modulation. This is primarily due to the difficulty in fabricating clean bcc-Cu(001) surfaces using conventional sputtering techniques.

In this study, we performed angle-resolved photoemission spectroscopy (ARPES) measurements on bcc-Cu/FeCo/MgO(001) thin films grown *in-situ* by molecular beam epitaxy (MBE) at the UVSOR BL7U beamline. The MgO(001) substrates were annealed at 500 °C for 60 minutes to clean the surface. The FeCo underlayer was deposited at a substrate temperature of 300 °C. The epitaxial growth of the FeCo layer and the cleanliness of the FeCo(001) surface were confirmed by low-energy electron diffraction (LEED) measurements (Fig. 1). Subsequently, a 1 nm-thick Cu layer was deposited at room temperature, and the formation of a clean bcc-Cu(001) surface was confirmed by LEED (Fig. 1). For comparison, an additional 20~ nm of Cu was deposited at room temperature to intentionally induce a structural transition to fcc-Cu, thereby fabricating fcc-Cu/FeCo/MgO(001) thin films. ARPES measurements were performed immediately after each deposition step.

Figure 2 (c)-(e) shows the ARPES results for FeCo(001), bcc-Cu(001), and fcc-Cu(001). ARPES measurements of FeCo ware performed at T = 250 K, ARPES measurements of bcc-Cu and fcc-Cu were performed at T = 15 K. Upon Cu deposition, a flat band attributed to Cu 3*d* electrons appeared near a binding energy = 2–3 eV. Furthermore, the electronic structure of Cu was found to be modulated as the film thickness increased. This modulation is considered to reflect the structural phase transition from the metastable bcc phase to the stable fcc phase. In addition, the spectra exhibited photon energy dependence, suggesting the presence of a three-dimensional electronic structure. These results not only provide fundamental insights into the electronic properties of bcc-Cu but also indicate the potential for tuning the electronic structure of Cu through thickness modulation.

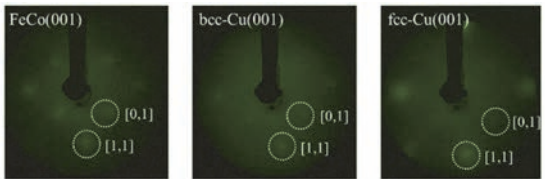

Fig. 1. LEED patterns of FeCo(001), bcc-Cu(001), fcc-Cu(001). Clean surfaces are observed respectively. All images are taken at incident electron beam energy = 210 eV.

[1] H. Li *et al*, Phys. Rev. B, **43**, (1991) 8.
[2] Z. Wang *et al*, Phys. Rev. B, **35**, (1987) 17.
[3] K. B. Fathoni *et al*., APL Mater., **7**, (2019) 111106.

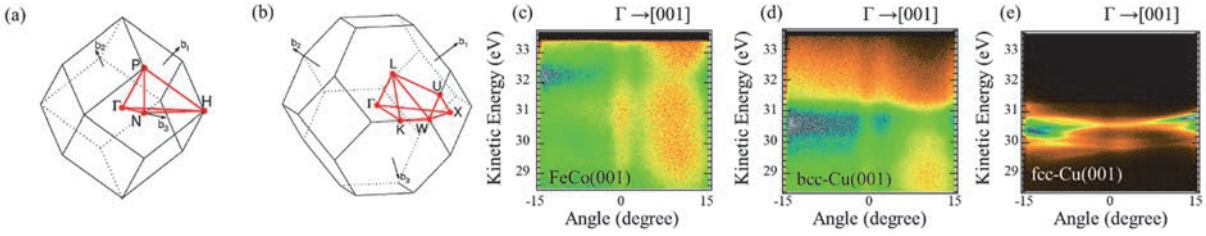

Fig. 2. (a) Brillouin zone of bcc lattice. (b) Brillouin zone of fcc lattice. (c)-(e)ARPES spectra of each sample along [001] axis. All spectra are measured at hν = 38 eV. Modulation of electronic states depending on the thickness of the Cu film was observed.

BL7U

Thin-Film Growth and Electronic Structure Study on YbSb/GaSb(110)

Y. Chen[1], T. Nakamura[2,1], R. Ichikawa[1], H. Yamaguchi[1], K. Nishihara[1], K. Tanaka[3] and S. Kimura[2,1,4]

[1]*Department of Physics, Graduate School of Science, The University of Osaka, Toyonaka 560-0043, Japan*
[2]*Graduate School of Frontier Biosciences, The University of Osaka, Suita 565-0071, Japan*
[3]*UVSOR Synchrotron Facility, Institute for Molecular Science, Okazaki 444-8585, Japan*
[4]*Department of Material Molecular Sciences, Institute for Molecular Science, Okazaki 444-8585, Japan*

Rare-earth mono-pnictide (*REPn*: *RE* = rare-earth element, *Pn* = pnictogen (Group V element)) exhibits a variety of magnetic properties, such as extreme magnetoresistance (XMR) reaching up to more than 10^6 % of the value at zero field [1], and a complicated magnetic phase transition in CeSb [2]. These characteristic physical properties originate from the hybridization between localized 4*f* orbitals in rare-earth elements and *p* orbitals in pnictogen elements, namely *p-f* mixing [3]. Recently, the existence of spin-polarized surface states in some *RE*Sbs and *RE*Bis [4] and the high-quality epitaxial thin-film grown by a molecular beam epitaxy (MBE) method were reported [5]. These novel studies lead us to anticipate possibilities as potential applications in spintronics devices. Meanwhile, despite the intense study on the *REPn* family, the knowledge of Yb mono-pnictides, such as YbSb, is still limited because of the difficulty in bulk single-crystal synthesis due to the high vapor pressure of Yb. We are focusing on the MBE growth and the electronic structure study on YbSb thin film. So far, we have tried the growth of YbSb thin film on the GaSb(001)-c(2×6) surface cleaned by Ar^+ sputtering and annealing. The obtained thin film shows an unexpected (2×1) reconstructed surface and a Fermi surface with 2-fold rotational symmetry [6]. Here, we fabricated YbSb thin films on another GaSb surface (110) to understand the origin of the anisotropy of YbSb/GdSb(001)-c(2×6).

To clarify the role of the surface-preparing method, we used two cleaning methods; one is Ar^+ sputtering at the substrate temperature of 720 K for 30 minutes, and the other is direct cleaving along the (110) plane. Yb and Sb were co-evaporated onto the cleaned substrates at 570 K with the flux-rate ratio of Yb and Sb as 1:1.1. Figure 1 shows LEED patterns measured after the deposition of YbSb for ~15 ML. For the thin-film growth on both substrates, streaks along the [001] direction with the same spacing as the diffraction spots of GaSb(110) on the [$\bar{1}$10] direction are observed. This result suggests that the substrate-preparing method is not essential for the sample quality.

Electronic structures of the differently prepared samples were detected with a synchrotron-based ARPES measurement. In the ARPES measurement, no clear dispersion could be observed along the [001] direction because of the lack of the long-range periodicity. On the other hand, as shown in Fig. 2, three hole bands and one electron pocket can be easily identified along the [$\bar{1}$10] direction for both substrates. The obtained ARPES image is consistent with the band calculation of YbSb [7] and the ARPES results of other *RE*Sbs [8]. These results suggest that the fabricated films are YbSb with a 1D-like growth along the [$\bar{1}$10] direction. One possible explanation could be dimer rows along the [$\bar{1}$10] direction form a staircase-like structure with two different heights along the [001] direction. Another possibility is that the obtained Yb-Sb thin film is a different compound, $YbSb_2$, reported in a recent paper [9]. To clarify the origin of the 1D-like feature, further detailed studies on chemical composition and crystallography by XPS and XRD are needed.

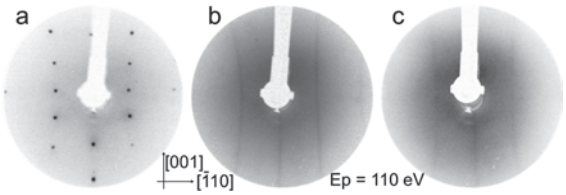

Fig. 1. LEED patterns of GaSb(110) cleaving surface (a), YbSb thin film growth on GaSb(110) substrates prepared by cleaving (b), and by Ar^+ sputtering (c), measured at 14 K.

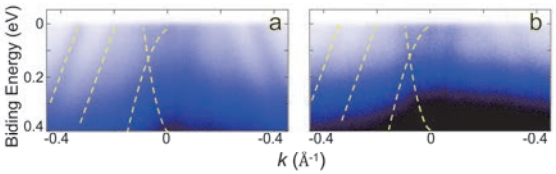

Fig. 2. ARPES intensity plots along the [$\bar{1}$10] direction and measured with 21-eV photons at 14 K of the YbSb thin-films growth on GaSb(110) substrates prepared by cleaving (a) and by Ar^+ sputtering (b).

[1] L. Ye *et al.*, Phys. Rev. B **97** (2018) 081108.
[2] J. Rossat-Mignod *et al*., J. Magn. Magn. Mater. **52** (1985) 111.
[3] H. Takahashi and T. Kasuya, J. Phys. C: Solid State Phys. **18** (1985) 2697, 2709, 2721, 2731, 2745, 2755.
[4] K. Kuroda *et al*., Phys. Rev. Lett. **120** (2018) 086402.
[5] S. Chatterjee *et al*., Phys. Rev. B **99** (2019) 125134.
[6] Y. Chen *et al*. UVSOR Activity Report **51** (2024) 164.
[7] X. Duan *et al*., Commun. Phys. **1** (2018) 71.
[8] P. Li *et al*., npj Quantum Mater. **8** (2023) 22.
[9] R. Dhara *et al*., Phys. Rev. Mater. **9** (2025) 034801.

BL7U

Observation of Electronic Structure of Chiral Magnet $GdNi_3Ga_9$ by ARPES

Y. Tanimoto[1], Y. Nakashima[1], H. Sato[2], K. Tanaka[3], S. Nakamura[4] and S. Ohara[4]
[1]*Graduate School of Advanced Science and Engineering, Hiroshima University, Higashi-Hiroshima 739-8526, Japan*
[2]*Hiroshima Research Institute for Synchrotron Radiation Science, Higashi-Hiroshima 739-0046, Japan*
[3]*UVSOR Synchrotron Facility, Institute for Molecular Science, Okazaki 444-8585, Japan*
[4]*Graduate School of Engineering, Nagoya Institute of Technology, Nagoya 466-8555, Japan*

Trigonal $GdNi_3Ga_9$ has a chiral crystal structure belonging to space group of *R*32 (No. 155) [1] and is of interest as a 4*f* chiral metallomagnetic compound [2]. The localized Gd 4*f* spins are magnetically ordered below T_N=19.5 K, forming an antiferromagnetic structure in the *ab*-plane, and exhibiting left- or right-handed helimagnetism with a propagation vector $\boldsymbol{q}$=(0, 0, 1.485) [2]. Spin-polarized conduction electrons are thought to be responsible for this phenomenon. $GdNi_3Ga_9$ has the same crystal structure as $YbNi_3Al_9$, the first discovered 4*f* chiral metallomagnetic compound [3]. $YbNi_3Al_9$ exhibits helimagnetism with $\boldsymbol{q}$=(0, 0, 0.82) [4], while ferromagnetic order in the *ab*-plane, in contrast to $GdNi_3Ga_9$. Thus, a comparative study for $GdNi_3Ga_9$ is expected.

We have previously performed angle-resolved photoemission spectroscopy (ARPES) on $YbNi_3Al_9$ and observed five hole-like Fermi surfaces around the $\overline{\Gamma}$ point and one electronic-like Fermi surface around the $\overline{K}$ point [5]. In this study, we conducted ARPES on $GdNi_3Ga_9$ to investigate the Fermi surface and band structure of conduction electronic states near the Fermi level (E_F). The experiments were carried out at BL7U of UVSOR-III using an electron analyzer (A-1, MB-Scientific). Single crystals for the ARPES measurements were synthesized by the flux-method using gallium as the solvent [2] and were cleaved *in situ* under an ultrahigh vacuum of ~5×10^{-9} Pa.

Figures 1(a) and 1(b) present ARPES intensity plots of $GdNi_3Ga_9$ measured at $h\nu$=24 eV with *p*-polarized and *s*-polarized geometries, respectively, along the $\overline{\Gamma}$-$\overline{M}$ direction of the surface Brillouin zone. Measurements were performed at 7 K, below T_N. At least three hole-like bands were observed around the $\overline{\Gamma}$ point in Fig. 1(a). On the other hand, Fig. 1(b) clearly shows two hole-like bands crossing E_F at k_x=0.3 and 0.5 Å^{-1}, as well as a convex-upward band around the $\overline{\Gamma}$ point. The shape of the observed bands closely resembles those of $YbNi_3Al_9$ [5].

Figures 2(a) and 2(b) show the Fermi surfaces of $GdNi_3Ga_9$ measured at $h\nu$=24 eV and *T*=7 K with *p*-polarized and *s*-polarized geometries, respectively. In Fig. 2(a), at least three hole-like Fermi surfaces, corresponding to the bands in Fig. 1(a), exhibit an approximately six-fold symmetry. In Fig. 2(b), two hole-like Fermi surfaces are observed, and that around k_x=0.4 Å^{-1} appears three-fold symmetric. The hole-like Fermi surfaces of $GdNi_3Ga_9$ appear larger compared to those of $YbNi_3Al_9$.

We have also measured ARPES spectra at 25 K above T_N. A remarkable change in the shape of the bands was not detected.

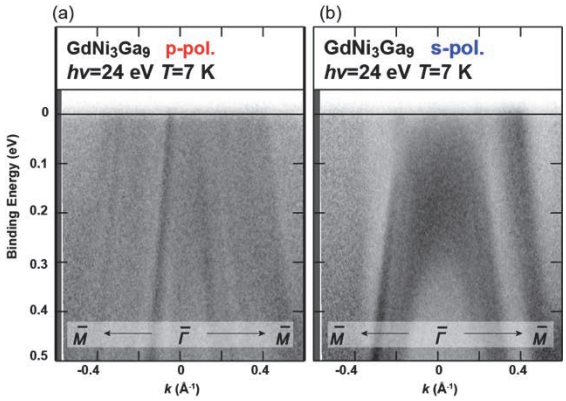

Fig. 1. ARPES intensity plots of $GdNi_3Ga_9$ measured along the $\overline{\Gamma}$-$\overline{M}$ direction at $h\nu$=24 eV and *T*=7 K with (a)*p*- and (b)*s*-polarized geometry.

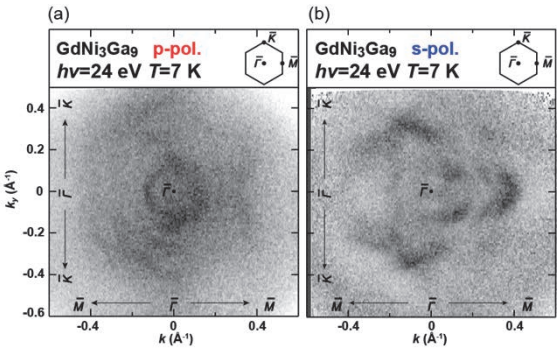

Fig. 2. The Fermi surfaces of $GdNi_3Ga_9$ measured at $h\nu$=24 eV and *T*=7 K with (a)*p*- and (b)*s*-polarized geometry.

[1] V. Topertser *et al*., Chem. Met. Alloys **12** (2019) 21.
[2] S. Nakamura *et al*., Phys. Rev. B **108** (2023) 104422.
[3] S. Ohara *et al*., JPS Conf. Proc. **3** (2014) 017016.
[4] T. Matsumura *et al*., J. Phys. Soc. Jpn. **86** (2017) 124702.
[5] Y. Tanimoto *et al*., in preparation.

BL7U

Photon Energy-dependent ARPES Study of Secondary Photoemission on $CaTiO_3$ and $BaTiO_3$

C.Z. Huang[1], C.Y. Hong[1], C.Y. Jiang[1,2], X.N. Zheng[1,2] and R.-H. He[1]
[1]*School of Science, Westlake Institute for Advanced Study, Westlake University, Hangzhou 310064, China*
[2]*Department of Physics, Fudan University, Shanghai 200433, China*

The discovery of the anomalous photocathode quantum material $SrTiO_3$ (STO) has garnered significant interest, yet the mechanism behind its extraordinary properties remains unclear[1]. Recently, a theoretical model introducing a novel Auger process that recycles secondary electrons and induces the emission of tertiary electrons has been proposed to explain the intense coherent photoemission in STO[2]. This model also predicts other perovskite oxides as candidate photocathode quantum materials and calls for further explorations.

As a technique that can directly probing the electronic structure of materials, Angle-resolved photoemission spectroscopy (ARPES) serves as a powerful tool for studying and discovering novel quantum materials. Photon energy-dependent ARPES measurements on STO have revealed that the intensity of the coherence peak is influenced by the excitation photon energy, with a threshold beyond which the peak intensity increases significantly[3]. $CaTiO_3$ (CTO) and $BaTiO_3$ (BTO), as perovskite oxides, are predicted to exhibit secondary photoemission characteristics similar to those of STO. Investigations into these materials may offer valuable insights into the mechanism underlying the exotic properties of these quantum materials.

Here, we report photon energy-dependent measurements on CTO and BTO thin films. The thin films were prepared by pulsed laser deposition and annealed at 1100-1200 ℃ for several hours to achieve clean surfaces for ARPES measurements. ARPES measurements were conducted at the BL7U beamline of UVSOR, utilizing photon energies ranging from 7.1 to 22 eV, with a sample temperature of 11 K.

Figure 1(a) shows the secondary photoemission spectrum (SPS) of CTO measured with photon energies ranging from 7.1 to 22 eV. The SPS peak at a kinetic energy of 4.3 eV remains nearly unchanged in position despite varying photon energy, while its intensity exhibits a clear photon energy dependence. As the photon energy increases to 8.1 eV, the peak intensity rapidly rises, reaching its maximum at a photon energy of 8.6 eV, and then begins to decrease. When the photon energy exceeds 12 eV, the peak intensity stabilizes.

For BTO, the variation of SPS peak intensity at a kinetic energy of 3.6 eV with photon energy follows a trend similar to that of CTO, exhibiting a threshold of 8.1 eV, a maximum of 8.8 eV, and stabilization above 12 eV.

The photon energy dependence of SPS peak intensity in CTO and BTO closely resembles that of STO, indicating a common origin for the anomalous secondary photoemission in these materials. Further investigations, such as examining the film thickness-dependence of SPS peak intensity, may provide more insights for understanding and utilizing these novel quantum materials.

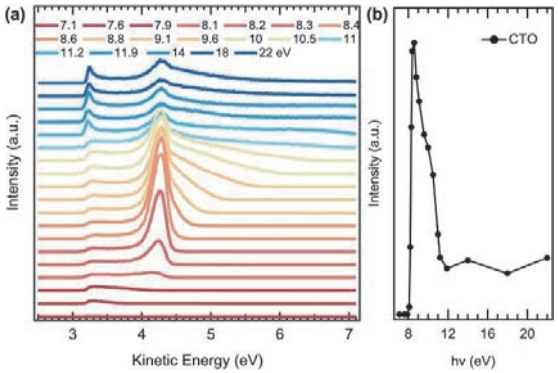

Fig. 1. (a) The secondary electron emission spectra of CTO measured with different photon energies. (b) The intensity of the peak at 4.3 eV as a function of photon energy.

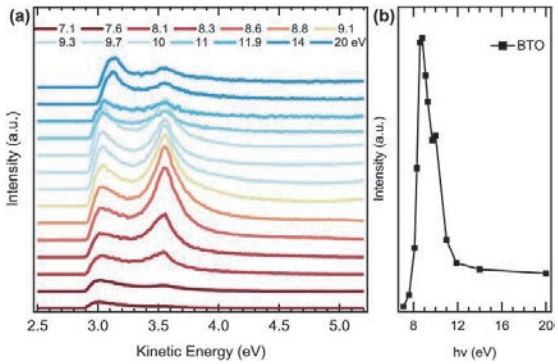

Fig. 2. (a) The secondary electron emission spectra of BTO measured with different photon energies. (b) The intensity of the peak at 3.6 eV as a function of photon energy.

[1] C. Hong *et al*., Nature **617** (2023) 493.
[2] M. Matzelle *et al*., arXiv:2405.06141 (2024).
[3] C. Hong *et al*.UVSOR Activity Report **51** (2023) 162.